Optics Letters

Demonstration of an imaging-free terahertz generation setup using segmented tilted-pulse-front excitation

Gergő Krizsán,[1,2,3,*] Gyula Polónyi,[2,3] Tobias Kroh,[4,5] György Tóth,[1,2] Zoltán Tibai,[1] Nicholas H. Matlis,[4] Gábor Almási,[1,2] Franz X. Kärtner,[4,5] and János Hebling[1,2,3]

[1] *Institute of Physics, University of Pécs, Ifjúság ú. 6, Pécs 7624, Hungary*
[2] *Szentágothai Research Centre, University of Pécs, Ifjúság ú. 20, Pécs 7624, Hungary*
[3] *ELKH-PTE High-Field Terahertz Research Group, Ifjúság ú. 6, Pécs 7624, Hungary*
[4] *Center for Free-Electron Laser Science CFEL, Deutsches Elektronen-Synchrotron DESY, Notkestr. 85, 22607 Hamburg, Germany*
[5] *The Hamburg Centre for Ultrafast Imaging, University of Hamburg, Luruper Chaussee 149, 22761 Hamburg, Germany*
*krizsan@fizika.ttk.pte.hu

A novel, to the best of our knowledge, compact, imaging-free, tilted-pulse-front (TPF) pumped terahertz (THz) source based on a LiNbO₃ slab with a small wedge angle (< 8°) and with an echelon microstructure on its input surface has been demonstrated. Single-cycle pulses of more than 40-μJ energy and 0.28-THz central frequency have been generated by 100-mJ, 400-fs pump pulses with 4.1×10^{-4} efficiency and excellent focusability. The peak electric field value focused by a single parabolic mirror was 540 kV/cm. Using 200-fs-long pump pulses, the efficiency increased to 1.0×10^{-3}, which is in qualitative agreement with the measured increased diffraction efficiency in the velocity matched diffraction order. A further ~8x increase in efficiency is expected by pumping a cryogenically cooled wedged echelon with appropriate step sizes, better microstructured surface quality, and antireflection coating on both the input and the output sides. THz generation efficiency maxima were found at ~2.7-mm crystal thickness for both pump pulse durations. The focused THz beam was diffraction limited within 5% accuracy. Compared to conventional THz sources, this setup is very compact, easy to align, can be pumped by larger beam sizes maintaining the high THz generation efficiency, and produces THz pulses with superior focusability.

Terahertz (THz) pulse applications, such as strong-field control of matter [1], charged particle manipulation, and acceleration [2–6], require the highest possible field strengths. To achieve that, high pulse energy and excellent focusability are essential.

Conventional tilted-pulse-front (TPF) setups using lithium niobate (LN) prisms have been providing the highest THz pulse energies in the low-frequency range of the THz spectrum. However, the scalability of such setups is limited by the following:

(i) limited interaction length due to angular dispersion [7]; (ii) imaging errors and pulse duration lengthening at the sides of a large pump beam [8]; and (iii) prism shape of the LN crystal with large (~63°) wedge angle [9]. In the past few years, several new setups were proposed to reduce or even eliminate these limitations [9–14]. In this Letter, we present the first experimental demonstration of an imaging-free wedged nonlinear echelon slab (NLES) THz source [9]. This setup significantly reduces limitation (i), eliminates (ii), and very strongly reduces (iii).

The investigated compact setup contains only two optical elements: a transmission grating (LightSmyth T-1600-1030s) used close to the Littrow configuration, and the wedged NLES. The scheme of the setup is illustrated in Fig. 1(a). The transmission grating introduces the pulse-front-tilt in air γ_0, which is smaller (~70°) than needed in a conventional setup (~77°). After diffraction off the grating, the pump beam propagates horizontally, then enters the wedged NLES perpendicularly to the surface of the echelon steps and becomes segmented. The tilt angle γ_{LN} of each pulse front segment is given by $\tan(\gamma_{LN}) = \tan(\gamma_0)/n_g$, where n_g is the group refractive index of the LN. The tilt angle γ of the average pulse front is given by the following equation:

$$\tan(\gamma) = \frac{\tan(\gamma_0)}{n_g} - \frac{\tan(\gamma_{slab})}{n_g} + \tan(\gamma_{slab}), \qquad (1)$$

where γ_{slab} is the tilt angle of the (average) front surface of the slab, and $\tan(\gamma_{slab}) = h/w$, where h and w are the horizontal and vertical size of the echelon steps, respectively. The generated THz radiation propagates perpendicularly to the average pulse front and can leave the NLES perpendicularly to its backside if the angle δ_w between the front and back surface is $\delta_w = \gamma - \gamma_{slab}$. Two different pump lasers were used in the THz generation experiments, both with 1030-nm central wavelength. The one with high energy (100 mJ used in the experiments) had a pulse duration of ~400 fs (FWHM) and its repetition rate was 52 Hz (Amplitude Magma). The pulses of the other laser had 1-mJ
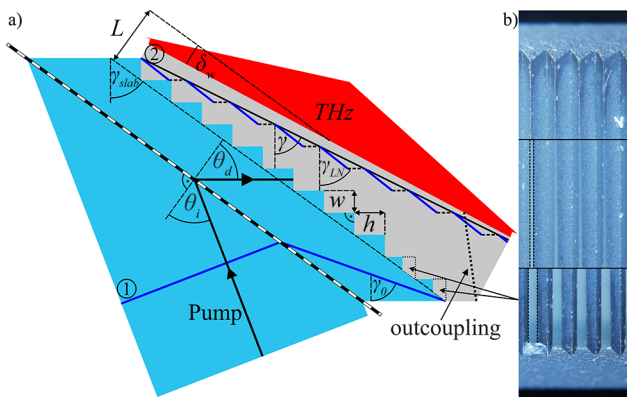
Fig. 1. (a) Scheme of the experimental setup. The snapshots of the pulse front are indicated by blue lines in the setup for two different times, indicated by ① and ②. Inside the wedged NLES the pulse front is segmented. (b) Microscope pictures of the microstructured surface's top, middle, and bottom parts. As can be seen, a significant part of the surface remained unstructured at the bottom. This unstructured portion becomes observable from 7 mm below the top of the slab. The unstructured parts are shown in between the dotted vertical lines.

maximal energy, 200-fs (FWHM) pulse duration, and 1-kHz repetition rate (Light Conversion Pharos SP-06-200-PP). In order to achieve the shortest pulse duration and the highest intensity inside the slab, which is necessary for efficient THz generation, the pump beam was pre-chirped by tuning the distance between the pulse compression gratings of the pump lasers.

A wedged 6% MgO-doped congruent LN slab with $\delta_w = 7.85°$ wedge angle (Wigner FK, Budapest, Hungary) was used. A microstructured entrance surface was created on it by diamond milling (Kugler GmbH., Salem, Germany). The dimensions of this surface were 20 mm perpendicular to and 34 mm in the plane of the drawing of Fig. 1(a), respectively. The slab average thickness was $L = 3.6$ mm. The width of the echelon steps, through which the pump beam entered the slab, was $w = 80\,\mu m$ [see Fig. 1(a)]. The height of the steps along the pump propagation direction was $h = 110.5\,\mu m$. These step sizes correspond to a γ_{slab} value of 54.1°. Such slab geometry was designed for working at cryogenic temperature, but for the sake of simplicity, this proof-of-principle experiment was performed at room temperature.

Figure 1(b) shows pictures taken from the top, middle, and bottom parts of the slab. As can be seen, on the middle and bottom parts the structuring was imperfect, and some of the surfaces remained unstructured. This problem occurred during the microstructuring process because the machining tool was not moving exactly parallel to the slab surface. The unstructured portion becomes observable starting from ~7 mm below the top of the slab. At the bottom of the crystal, only ~58% of the surface was microstructured. Additionally, the structured surface contained manufacturing defects (holes and breakdowns) in a significant part of the area (~25%). According to optical microscope measurements (Olympus DSX510), the surface roughness S_a measured on a $30 \times 30\,\mu m$ defect-free area was ~100 nm. This leads to some scattering of the pump and reduces the diffraction efficiency of the microstructure.

To quantitatively describe the microstructure quality, diffraction efficiency measurements were performed. For this purpose,

the thick side of the wedged NLES was cut to efficiently outcouple a small diameter beam. This new surface is indicated by a dotted line and "outcoupling" in Fig. 1(a). The well-structured surface (top side) of the wedged NLES was directly (in the absence of the transmission grating) illuminated at the thicker end of the wedged NLES by the Pharos pump laser (200 fs) and by a CW Yb laser (CrystaLaser CL1030-200), respectively. After the diffraction from the microstructure, the beams left the crystal through the "outcoupling" surface. The pump beam energy was measured just before and after the wedged NLES. In the case of perfect microstructure quality (smooth step surfaces without defects), considering the Fresnel reflections on the entrance and exit surfaces, the total transmitted energy (all orders together) should be ~74%. Instead, the measured total transmitted energy was 53% (38.9%) using the 200-fs (CW) beam. The main diffraction order should contain ~90% (~80%) of the transmitted energy for the two types of lasers, respectively. Instead, the measured energy in the main order contained only 70% (52%) energy of the beam. According to these results, with increasing microstructure quality, up to 1.8 (2.9) times higher energy can be expected in the main diffraction order in case of short (long) pump pulse duration. With this, the THz generation efficiency would increase at least proportionally.

The difference between the diffraction efficiencies for the two types of lasers arises from the different diffraction mechanisms of the microstructure. If the pulse duration is shorter than τ_d, the difference in time required for the light to propagate over the length of the microstructure depth h inside LN and air, respectively, no interference can occur between the neighboring pulse front segments. In this case, diffraction by the microstructure can be considered as diffraction from individual slits. However, if the pulse duration is longer than τ_d, the microstructure works as a high-order blazed transmission grating. For the present wedged NLES, τ_d is calculated to be $\tau_d = h(n_g - 1)/c = 424$ fs, where c is the speed of light. Here we would like to note that at least partial interference is occurring between the different pulse front segments in the case of the high-energy laser beam because its Fourier-limited pulse duration is ~680 fs ($1/e^2$) and the pulse was pre-chirped, which further elongates it.

The angle of incidence onto the grating was measured carefully by referencing it to the retro-reflected beam at normal incidence. From the measured incidence angle, the diffraction angle of the optical grating was calculated. Once the angle between the grating and the wedged NLES is known, the angle of incidence onto the echelon structure and the beam size on it, γ and γ_{LN}, can be easily calculated, too.

In the THz generation experiments, the setup was optimized for THz energy. The optimum was found in a geometry when the grating was aligned parallel to the surface of the wedged NLES. The optimized setup parameters for the two pump sources are listed in Table 1, where τ_p is the pump pulse duration, and θ_i and θ_d are the angles of the beam incident and diffracted by the optical grating, respectively. We would like to note that Fig. 1(a) illustrates the geometry corresponding to the 200-fs pump pulse scenario. The difference between the optimum configurations found are, again, related to the pulse duration of the laser pulses used. Shorter pulses allow for generation of higher THz frequencies, which requires a larger pulse-front-tilt angle to maintain phase-matching (last column in Table 1). Simultaneously, higher THz conversion efficiency can be expected.

Figure 2 highlights the compactness of the setup, which is smaller than the THz detector.

The dependence of the conversion efficiency on the slab thickness and the microstructure quality was investigated with both pump sources. In these experiments, the beam size of the 200-fs (400-fs) pump pulse was ∼ 2.3×2.8 mm (2.3×4.5 mm) diameter ($1/e^2$) along horizontal and vertical dimensions, respectively. Figure 3 shows how the THz generation efficiency depends on the crystal thickness for the 200-fs pump laser. For each thickness value, the pre-chirp of the pump was optimized individually. We want to point out that once the pre-chirp was set for the average thickness, only a small increase in efficiency ($<2\%$) was observed by further optimization at other thickness values. According to Fig. 3, the optimal crystal thickness is ∼2.7 mm. The local minimum observed for a thickness of around 2.2 mm most likely is caused by a local, reduced microstructure quality. The measurement with the 400-fs pump showed a similar dependence on the crystal thickness, but the THz generation efficiency was less than half compared to the use of the 200-fs pump. The peak fluence and intensity in Fig. 3 are given for the entrance of the NLES, and the latter is calculated assuming Fourier-limited pulse duration.

The THz generation efficiency was observed to correlate with the microstructure quality: setting the pump onto the bottom of the wedged NLES, where only a fraction (∼58%) of the slab was well-structured, reduced the generated THz energy by approximately the same amount (∼57.5%) compared to the position at the top.

Pumping the better microstructured part of the wedged NLES with a ∼16.7×13.6-mm beam size and 100-mJ energy, ∼41-μJ THz pulses were generated with 0.041% efficiency. The THz generation characteristic can be seen in Fig. 4. The efficiency scales almost linearly with the pump energy within the interval scanned in the experiment. Between the wedged NLES and the calibrated pyroelectric THz detector (Sensor und Lasertechnik, THz 20), a Teflon plate and black paper were used to filter out the scattered pump beam. The THz transmission value of these filters was carefully measured and taken into account for the THz energy measurement. Here we would like to note that the horizontal size of the wedged NLES THz output (34 mm) was

Table 1. Optimized Setup Parameters for the Two Different Pump Pulse Durations

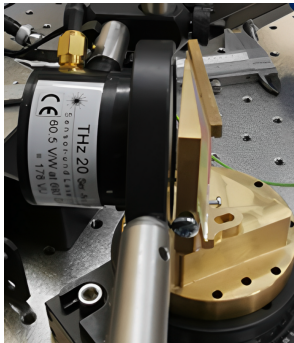| τ_p (fs)	θ_i (°)	θ_d (°)	γ_0 (°)	γ_{LN} (°)	γ (°)
200	57	54.0	70.4	51.8	63.7
400	61	50.6	69.0	49.6	62.7

Fig. 2. Picture of the experimental setup. From left to right: THz detector (including black paper), Teflon filter, wedged NLES, transmission grating.
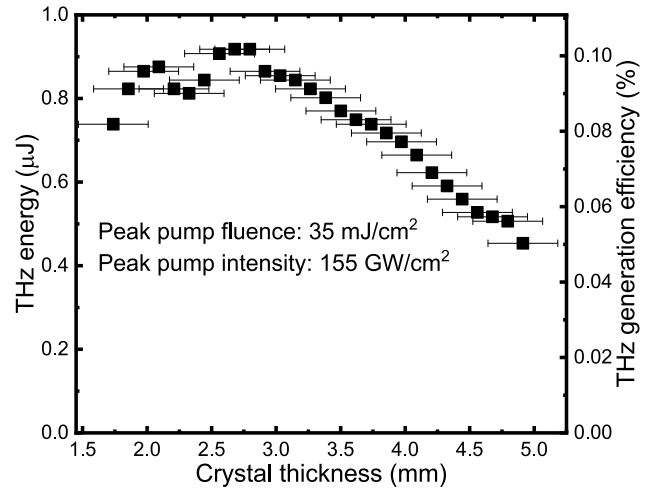

Fig. 3. THz generation efficiency versus the crystal thickness measured with 200-fs pump pulses. The horizontal error bar represents the horizontal beam size.
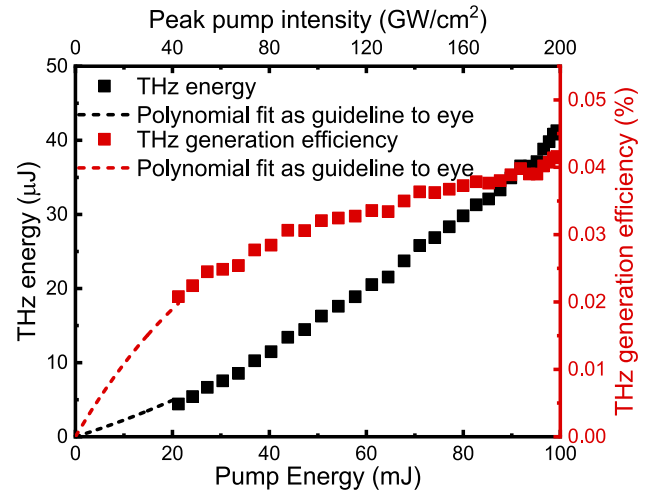

Fig. 4. Generated THz energy and generation efficiency dependence on the pump energy and intensity using the high-energy pump (400 fs).

larger than the detector size (20 mm), such that the real THz energy is in fact underestimated by the measurement.

Figure 5 shows the electro-optically sampled E-field of the generated THz pulse. For the electro-optic sampling, a 1-mm-thick gallium phosphide crystal with (110) orientation was used, while a small portion of the pump beam was used as the probe beam. The amplitude of the electric field was calculated to be 540 kV/cm based on the measured THz beam profile (left inset of Fig. 5), the waveform, and the pulse energy. The corresponding THz spectrum is shown in the right inset of Fig. 5. The central frequency was 0.28 THz and the spectral FWHM was 0.38 THz. This relatively low center frequency is caused by the long pump pulse duration in combination with the increasing THz absorption toward higher frequencies in LN at room temperature, and by the dephasing effect of the segmented pulse front. Furthermore, the actual signal is convolved with the temporal profile of the probe pulse, which leads to a reduced resolution at higher
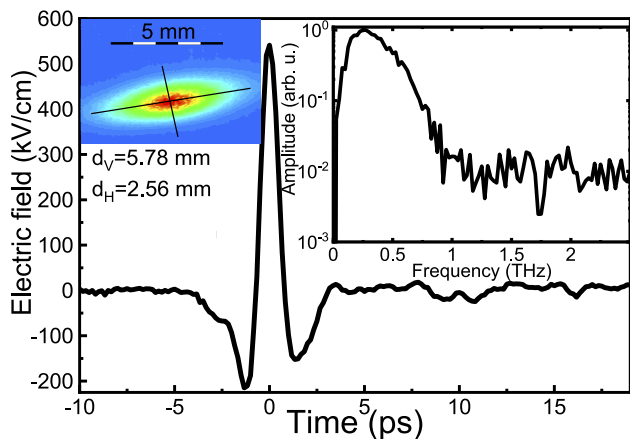
Fig. 5. THz waveform measured by electro-optical sampling. Inset left: Focused THz beam size measured with a Pyrocam IV THz camera. Inset right: THz spectrum calculated from the waveform.

frequencies and thus shifts the measured center frequency by about 10% toward lower values.

In the left inset of Fig. 5, the measured THz beam focused by a single off-axis parabolic mirror (3-inch diameter and 3-inch focal length) placed 150 mm from the wedged NLES is shown. A minimum THz beam cross section of 2.5×4.3 mm ($1/e^2$) in diameter in horizontal and vertical directions, respectively, was observed at a distance of 76 mm from the focusing mirror. Note that the THz beam showed slight astigmatism. During the high-energy experiments, three different vertical pump beam sizes were used—4.5, 6.79, and 9.03 mm—and the measured focused THz beam sizes were in good agreement with the calculated one (within a 5% error). For the calculations, a Gaussian beam was assumed with the spectrum calculated from the measured THz waveform. For every spectral component, the beam waist was assumed to align with the output side of the slab. Its sizes were estimated to be equal to the crystal size horizontally (34 mm) and the actual pump beam size vertically. Then the beam waists were imaged with one focusing element of 3-inch focal length. The focused beam size was determined from the weighted sum of the individual spectral components. The ellipticity of the focused THz beam originates from the opposite ellipticity of the pump beam. In general, the larger beam has smaller divergence and can be focused down to smaller sizes, which is especially useful for THz beams at relatively long wavelengths.

In conclusion, a compact THz pulse source generating more than 40 μJ of THz energy with 0.04% efficiency at 0.28-THz central frequency has been demonstrated. Using shorter pump pulse durations than τ_d resulted in higher diffraction efficiency and higher THz generation efficiency. Using a pump with a 200-fs pulse duration increased the generation efficiency to 0.1%. This edification can be applied to other sources where a microstructure is created in the nonlinear material surface. The optimal thickness of the LN was found to be ~2.7 mm. This experimental result is useful for the authentication of theoretical models or for THz source designing, especially selecting the slab thickness in case of plane-parallel setups. Here we would like to note that the optimal thickness is expected to decrease for shorter pulse durations according to the scaling of the optimum interaction length. The THz pulses generated by this wedged NLES setup have exceptionally good focusability, which is required by many high-field applications, such as particle acceleration. The THz generation efficiency of the demonstrated wedged NLES source is lower than that reported for current conventional TPF-based ones. However, its performance is expected to improve more than an order of magnitude by implementing the following changes: cryogenic cooling (2x); use of stochiometric LN (1.3x); refined microstructure quality (1.8x); pumping with high intensity, short ($< \tau_d$) pulses (2.5x); applying antireflection coating to the front side for the pump (1.12x) and at the backside for THz beam (1.5x). Such an improved wedged NLES structure, if scaled in size accordingly, could be used to generate THz pulses of unprecedented energy and quality. For example, a 34-mm-sized structure pumped by a ~500-mJ, 200-fs, 1030-nm pulse with flattop profile is expected to yield THz pulses with an energy of ~4 mJ (0.8% conversion efficiency). The expected peak field obtained at the focus of a single off-axis parabolic mirror exceeds 7 MV/cm, which can be used for many high-field experiments, including free-space particle acceleration.

Disclosures. The authors declare no conflicts of interest.

Data availability. The data that support the findings of this study are available within the article and from the corresponding author upon reasonable request.

REFERENCES

1. P. Salén, M. Basini, S. Bonetti, J. Hebling, M. Krasilnikov, A. Y. Nikitin, G. Shamuilov, Z. Tibai, V. Zhaunerchyk, and V. Goryashko, Phys. Rep. **836-837**, 1 (2019).
2. D. Zhang, A. Fallahi, M. Hemmer, X. Wu, M. Fakhari, Y. Hua, H. Cankaya, A.-L. Calendron, L. E. Zapata, and N. H. Matlis, Nat. Photonics **12**, 336 (2018).
3. E. Curry, S. Fabbri, J. Maxson, P. Musumeci, and A. Gover, Phys. Rev. Lett. **120**, 094801 (2018).
4. M. T. Hibberd, A. L. Healy, D. S. Lake, V. Georgiadis, E. J. Smith, O. J. Finlay, T. H. Pacey, J. K. Jones, Y. Saveliev, and D. A. Walsh, Nat. Photonics **14**, 755 (2020).
5. Z. Tibai, S. Turnár, G. Tóth, J. Hebling, and S. W. Jolly, Opt. Express **30**, 32861 (2022).
6. D. Zhang, Y. Zeng, M. Fakhari, X. He, N. H. Matlis, and F. X. Kärtner, Appl. Phys. Rev. **9**, 031407 (2022).
7. J. Fülöp, L. Pálfalvi, G. Almási, and J. Hebling, Opt. Express **18**, 12311 (2010).
8. L. Tokodi, J. Hebling, and L. Pálfalvi, J. Infrared, Millimeter, Terahertz Waves **38**, 22 (2017).
9. G. Tóth, L. Pálfalvi, J. A. Fülöp, G. Krizsán, N. H. Matlis, G. Almási, and J. Hebling, Opt. Express **27**, 7762 (2019).
10. B. K. Ofori-Okai, P. Sivarajah, W. R. Huang, and K. A. Nelson, Opt. Express **24**, 5057 (2016).
11. L. Pálfalvi, Z. Ollmann, L. Tokodi, and J. Hebling, Opt. Express **24**, 8156 (2016).
12. L. Pálfalvi, G. Tóth, L. Tokodi, Z. Márton, J. A. Fülöp, G. Almási, and J. Hebling, Opt. Express **25**, 29560 (2017).
13. G. Tóth, L. Pálfalvi, Z. Tibai, L. Tokodi, J. A. Fülöp, Z. Márton, G. Almási, and J. Hebling, Opt. Express **27**, 30681 (2019).
14. L. Guiramand, J. Nkeck, X. Ropagnol, T. Ozaki, and F. Blanchard, Photonics Res. **10**, 340 (2022).